Songklanakarin J. Sci. Technol.
37 (6), 683-690, Nov. - Dec. 2015

http://www.sjst.psu.ac.th

Original Article

Effects of cyclic shear loads on strength, stiffness and dilation of rock fractures

Thanakorn Kamonphet, Supattra Khamrat, and Kittitep Fuenkajorn*

Geomechanics Research Unit, Institute of Engineering,
Suranaree University of Technology, Mueang, Nahkon Ratchasima, 30000 Thailand.

Received: 9 October 2014; Accepted: 9 July 2015

Abstract

Direct shear tests have been performed to determine the peak and residual shear strengths of fractures in sandstone, granite and limestone under cyclic shear loading. The fractures are artificially made in the laboratory by tension inducing and saw-cut methods. Results indicate that the cyclic shear load can significantly reduce the fracture shear strengths and stiffness. The peak shear strengths rapidly decrease after the first cycle and tend to remain unchanged close to the residual strengths through the tenth cycle. Degradation of the first order asperities largely occurs after the first cycle. The fracture dilation rates gradually decrease from the first through the tenth cycles suggesting that the second order asperities continuously degrade after the first load cycle. The residual shear strengths are lower than the peak shear strengths and higher than those of the smooth fractures. The strength of smooth fracture tends to be independent of cyclic shear loading.

Keywords: shear strength, asperity, fracture stiffness, dilation, cyclic loading

1. Introduction

Joint shear strength is one of the key properties used in the stability analysis and design of engineering structures in rock mass, e.g. slopes, tunnels and foundations. The conventional method currently used to determine the joint shear strength is the direct shear testing (e.g. ASTM D5607-08). The joint properties, such as roughness, strength of asperities, separation, gouge and even the spatial distributions make the behavior of jointed rock masses more complicated (Lee *et al.*, 2001). Most of the previous laboratory experiments on the mechanical properties of rock joints have been focused on determining the peak shear strength and the stress–displacement relations under unidirectional shear loading. Cyclic displacements due to earthquake loadings can however affect the shear strength. The cyclic effect has been first recognized by Hutson and Dowding (1990) who conclude that the cyclic shear loading can reduce the shear strengths of rock fractures. Jafari *et al.* (2002, 2003) have performed shear testing on rock replica fractures (cast cement) to investigate the effect of cyclic shear loading on the degradation of fracture asperities. They propose an empirical model to describe the fracture shear strength as affected by number of shear cycles. The model is then compared with some shear test results from the actual rock fractures. Hosseini *et al.* (2004) stated that small repetitive earthquakes may not make considerable movements, but because of their repetitive nature they may affect the shear resistance of rock joints. These cyclic displacements can degrade the first and second order asperities along the joint surface and reduce its shear strength. The shear strength of rock joints under cyclic loadings is therefore an important consideration for long-term stability of engineering structures in the areas where seismic activities occur. Even though the cyclic shear effect has long been recognized data basis relevant to the issue have rarely been produced. In particular, the effects of cyclic shear load on the fracture stiffness, dilation rate, and on different fracture roughness have rarely been investigated.

The objective of this study is to investigate the rock fracture strength and stiffness under cyclic shear loads in the laboratory. The effort primarily involves performing series

* Corresponding author.
Email address: kittitep@sut.ac.th

of cyclic direct shear tests on smooth and rough fractures. The peak and residual shear strengths, fracture shear stiffness, dilation rate and degradation of asperities of the fractures under cyclic shearing are of interest. The findings are of useful in understanding the shear behavior of rock fractures as affected by cycles of shear loading.

2. Rock Samples

The rocks selected for this study are Phu Phan sandstone, Saraburi limestone, and Tak granite (hereafter called PPSS, SLS and TGR). The sandstone is fine grained rock brownish yellow and composed mainly of quartz and feldspar with a few mica. They are well sorted and angular. The rock comprises 72% quartz (0.2-0.8 mm), 20% feldspar (0.1-0.8 mm), 3% mica (0.1-0.3 mm), 3% rock fragment (0.5-2 mm), and 2% other (0.5-1 mm). The limestone is rounded pelsparite texture. The rock comprises 97% calcite, 0.57% dolomite, 0.94% quartz and 0.6% clays. Tak granite is felsic and phaneritic rock. It comprises 40% plagioclase (0.5-1 mm), 30% quartz (2-5 mm), 5% orthoclase (3-5 mm), 3% amphibole (1-2 mm), and 2% biotite (1-2 mm).

The block specimens are prepared to have nominal dimensions of 10´10´16 cm. Specimens with smooth fracture are simulated by using saw-cutting surfaces. The rough surfaces are prepared by applying a line at the mid-section of the specimens until splitting tensile failure occurs (tension-induced fractures). For both smooth and rough fracture specimens, the upper block is trimmed out about 1 cm to obtain constant contact area during shearing. The tested fracture area is 9´10 cm. Figure 1 shows examples of rock fractures prepared for the three rock types. The asperity amplitudes on the fracture planes are measured using the laser-scanned profiles along the shear direction (Figure 2). The readings are made to the nearest 0.01 mm. The maximum amplitudes can be used to estimate the joint roughness coefficients (JRC) of each fracture based on Barton's chart (Barton, 1982). The initial JRC values for the fractures in sandstone, limestone and granite are in the ranges of 8-10, 10-12 and 18-20. The roughness of the tension-induced fractures tends to be governed by the textures and mineral compositions of the rocks. Hence, the fracture roughness for each rock type is in the narrow range of the JRC values (i.e. tends to remain constant). The rock density is measured using the ASTM (C 127-12). The densities of sandstone, limestone and granite specimens are 2.31, 2.85 and 2.71 g/cc. These rocks are classified as medium to strong rocks based on the ISRM standard (Brown, 1981). The rock uniaxial compressive strengths determined from previous studies are 85, 93 and 118 MPa for Phu Phan sandstone (Fuenkajorn and Khenkhonthod, 2010), Saraburi limestone (Boonbatr and Fuenkajorn, 2011),

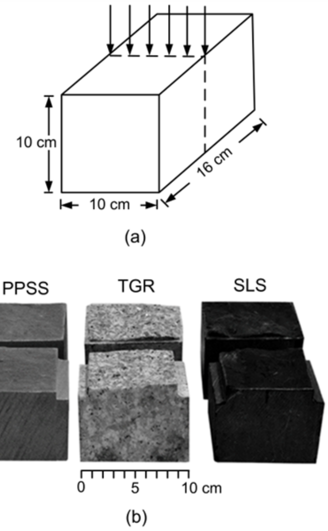

Figure 1. Line load applied at the mid-section of the specimens to obtain a tension-induced fractures (a), and tension-induced fractures specimens (b).

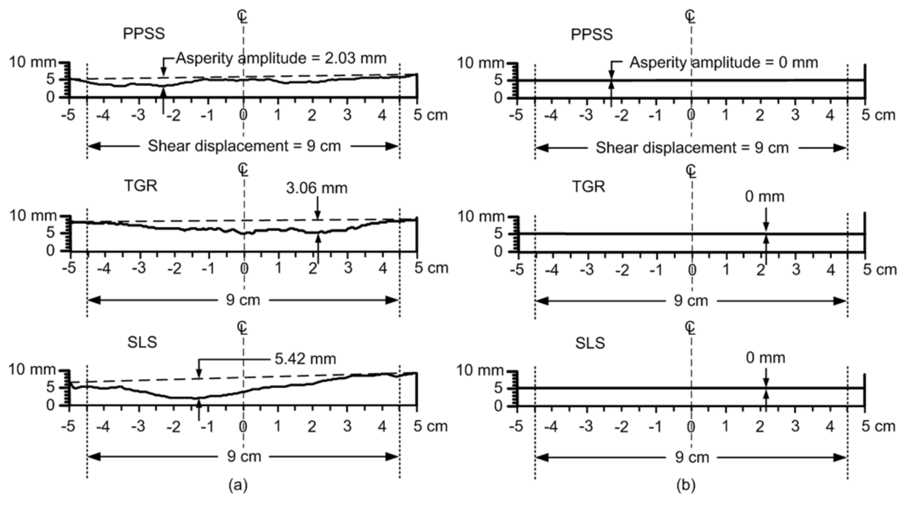

Figure 2. Examples of laser-scanned profiles revealing the maximum asperity amplitude used to estimate the joint roughness coefficient (JRC) for tension-induced fractures (a) and smooth saw-cut surfaces (b).

and Tak granite (Rodklang and Fuenkajorn, 2014). These selected rock samples are highly uniform in texture and mechanical properties, and hence the study performed here is isolated from the effects of the intrinsic variability due to the non-homogeneity for each rock type.

3. Test Method

The test method and calculation follow as much as practical the ASTM (D5607-08) standard practice. Each specimen is sheared under each normal stress using a direct shear device (SBEL DR44) (Figure 3). The applied constant normal stresses are 0.5, 1, 2, 3, and 4 MPa. The rates of shear displacement are maintained constant at 0.01-0.02 mm/s. The maximum number of loading cycles is 10 with the maximum shear displacement of ±5 mm (forward and backward), which is equivalent to the amplitude of 10 mm. The applied normal and shear forces and the corresponding normal and shear displacements are monitored and recorded. Linear variable differential transformers (LVDT's) are used to measure the shear and normal displacements. Each loading cycle is divided into four stages: forward advance (stage I) when the specimen moves from the center to +5 mm with positive corresponding shear stress; forward return (stage II) when the specimen returns from +5 to the center with negative shear stress; backward advance (stage III) when the specimen moves from the center to -5 mm with negative corresponding shear stress; backward return (stage IV) when the specimen returns from -5 to the center with positive shear stress (Figure 4). Due to the limitation of the available shear device and measurement system the cyclic frequency is relatively low, about 10^{-3} cycle/second. The effect of cyclic frequency is not investigated in this study

4. Test Results

The shear stresses are calculated and presented as a function of shear displacement for each constant normal stress. Figure 5 shows examples of shear stress-displacement curves under 0.5 MPa (minimum) and 4 MPa (maximum) normal stresses. For all rock types the first shear cycle clearly reveals the peak shear and residual shear stresses under each normal load. From the second to tenth cycles, the peak shear stress rapidly reduces to close to the residual shear values. Under low normal stress the residual shear stresses remain virtually unchanged for all cycles. Under high normal stresses however the residual shear stresses continue to decrease slightly as the number of shear cycles increase. This observation is more obvious for strong rock (granite) than for softer rock (sandstone). The reduction of the peak shear stresses under the first shear cycle is due to the degradation of the first order asperities. The residual shear stresses are contributed by the shearing resistance of the second order asperities, which gradually decrease as the shear cycles increase. This conclusion is supported by the results of the fracture dilation rate (vertical-to-horizontal displacement ratio)

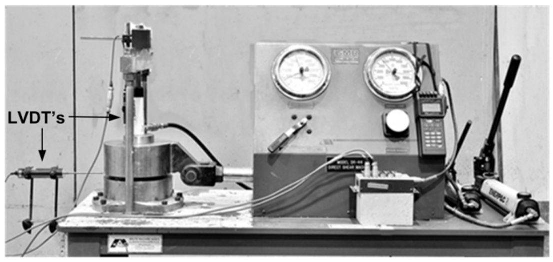

Figure 3. Direct shear device SBEL DR44 used in this study.

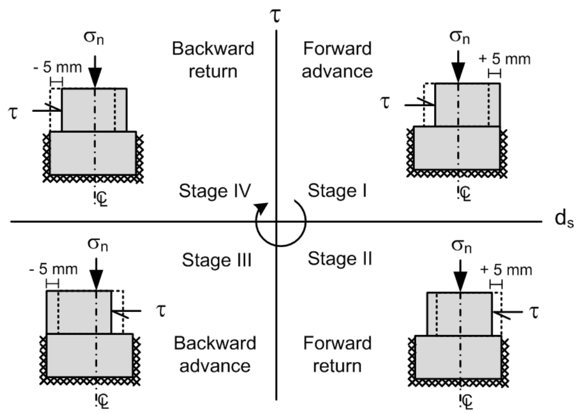

Figure 4. Shearing paths for four stages in one cycle.

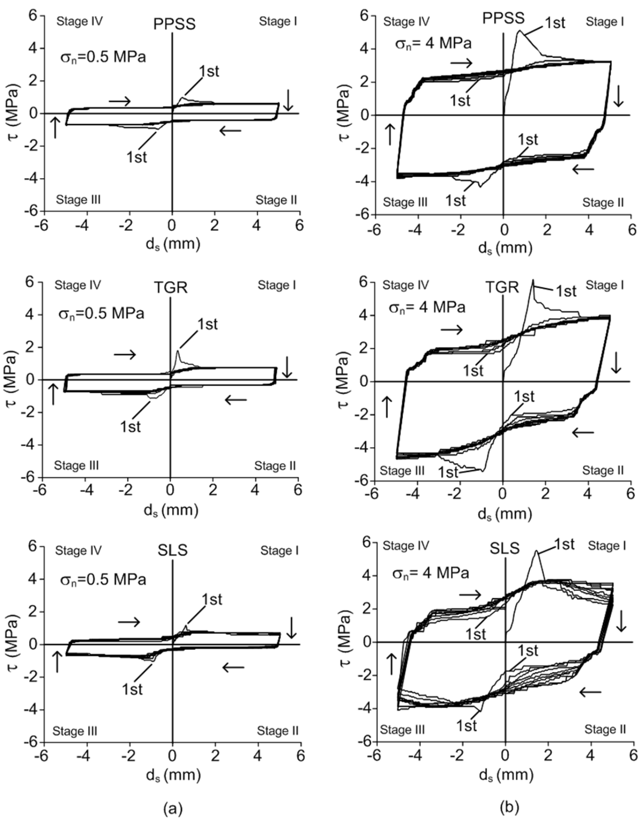

Figure 5. Examples of shear stress-displacement curves for tension-induced fracture specimens under normal stresses of 0.5 MPa (a) and 4 MPa (b).

monitored during shearing. Figure 6 shows examples of the dilation as a function of shear displacement on the tension-induced fractures under 0.5 MPa and 4 MPa normal stresses. The dilation rapidly decreases after the first shear cycle due to the sheared-off of the first order asperities. Then it gradually decreases as the shear cycles increase, which is probably due to the slow degradation of the second order asperities. The dilation rates (d_n/d_s) are plotted as a function of number of shear cycles in Figure 7. The diagrams clearly show the reduction of dilation rates as the shear cycles and normal stresses increase.

Figure 8 shows the shear stress-displacement curves of the smooth saw-cut fractures under 0.5 MPa and 4 MPa normal stresses. No peak shear stress is detected for all normal loads and loading cycles. The results from cycle one to cycle ten are virtually identical. This suggests that the shear strengths and dilation rates of the smooth fracture are independent of the shear cycle.

Figure 9 shows the fracture shear stiffness values (K_s) calculated for all cycles of the three rock types. Fracture shear stiffness is the parameter defined as the slope at a linear portion of the shear stress-displacement curve before the peak value is reached (Jaeger *et al.*, 2007). It represents the ratio of shearing stress-to-deformation of a fracture before any significant displacement occurs. The results (data points in Figure 9) indicate that the shear stiffness of the tension-induced fractures rapidly drops during the first few

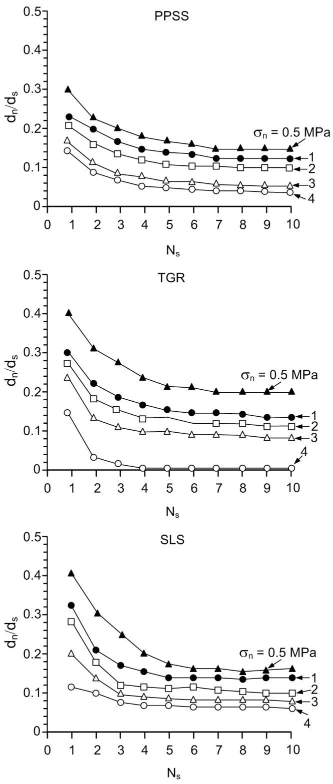

Figure 7. Dilation rate (d_n/d_s) as a function of number of shear cycles (N_s).

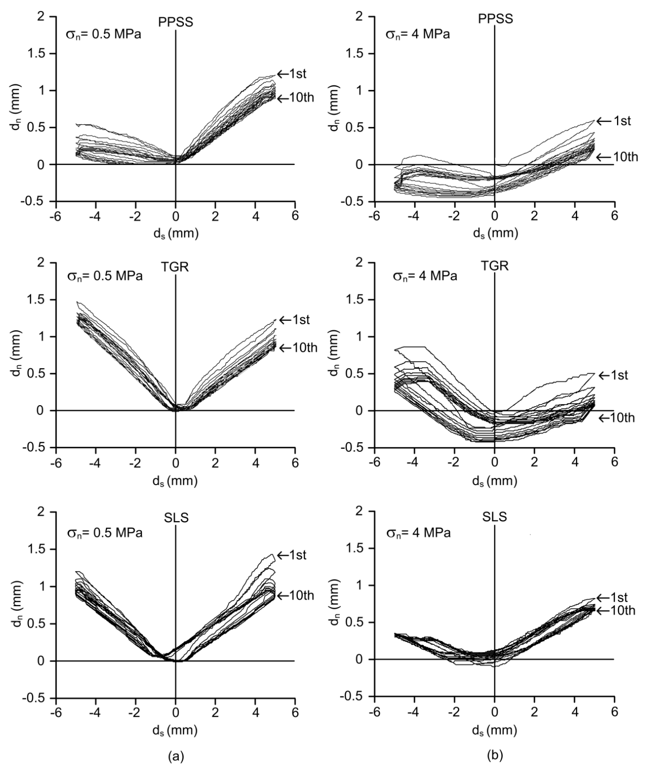

Figure 6. Normal displacement as a function of shear displacement for tension-induced fractures under normal stresses of 0.5 MPa (a) and 4 MPa (b).

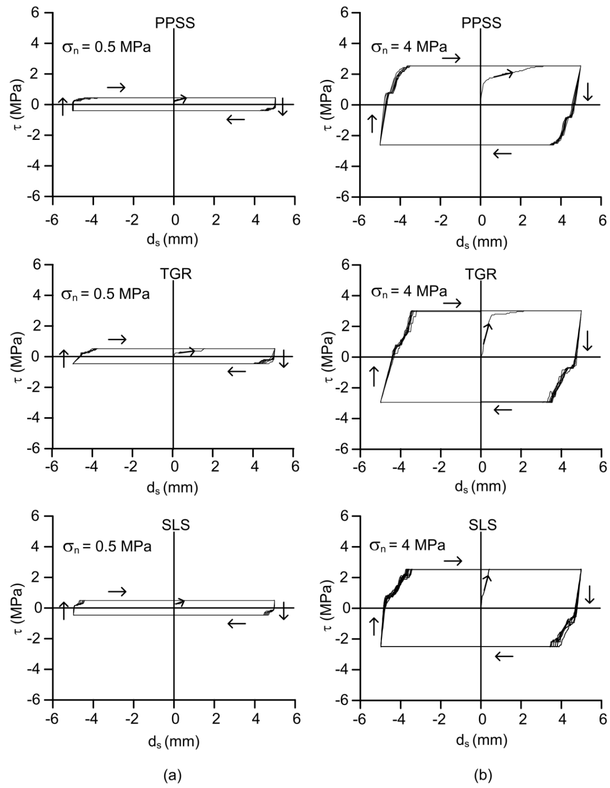

Figure 8. Examples of shear stresses as a function of shear displacement for smooth saw-cut surfaces under normal stresses of 0.5 MPa (a) and 4 MPa (b).

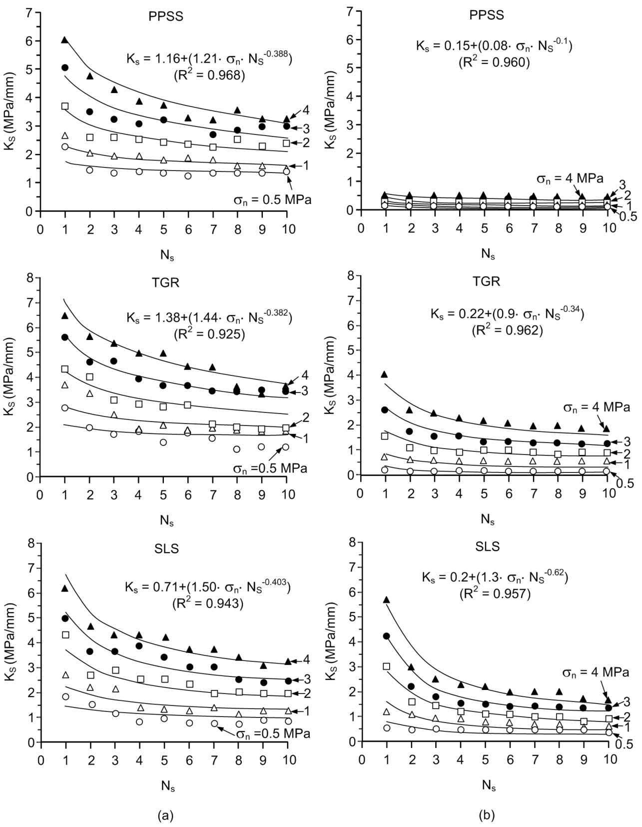

Figure 9. Joint shear stiffness (K_s) as a function of number of shear cycles (N_s) for tension-induced fractures (a) and smooth saw-cut surfaces (b).

shear cycles, and then gradually decreases and approaching a limit value near the tenth shear cycle for each normal load. The larger decrease is observed under the greater normal load. The shear stiffness for smooth fractures is also determined. Their values from the sandstone are significantly lower than those of the rough fractures. For granite and limestone, the shear stiffness values of the smooth fractures are slightly lower than those of the rough fractures. This is probably due to that the cohesive force at the contacts of smooth surfaces for the granite and limestone are greater than that of the sandstone. More discussion on this issue is given in the next section.

An empirical equation is proposed here to represent the fracture shear stiffness as a function of normal stress (σ_n) and number of shear cycles (N_s). After several trials, it is found that the power equation can best represent the reduction of the shear stiffness as σ_n decreases and N_s increases. It can be described as follows:

$$K_s = \alpha + \{\beta \times \sigma_n \times N_s^{\kappa}\} \quad (1)$$

where α, β and κ are empirical constants. Linear regression analyses have been performed on the test data using SPSS statistical software (Wendai, 2000) to determine these empirical constants. The results are shown in Figure 9 for both tension-induced and smooth fractures. Good correlations are obtained between the test data and the proposed equation (R^2 is greater than 0.9). Equation (1) is useful to predict the shear stiffness (K_s) of the tested fractures in Tak granite, Phu Phan sandstone and Saraburi limestone. The fracture roughness is not explicitly incorporated into the above equation. This is primarily because the tension-induced fractures tend to be consistent for each rock type.

Post-test measurements of the JRC values have been made after the 10th-cycle (Table 1). The differences of the JRC values between the 1st cycle and 10th cycle are larger for the sandstone, compared to those of the granite and limestone. This is probably because the sandstone has the lowest strengths than the other two.

5. Strength Criterion

An attempt is made here to demonstrate how the shear cycles affect the fracture strength under various normal loads, and hence suitable strength criterion can be developed and applied to the stability analysis and design of engineering structures in rock mass. The Coulomb shear strength criterion is adopted here to describe the fracture shear strength (τ) as a function of normal stress (σ_n) as follows (Jaeger *et al.*, 2007):

$$\tau = c + \sigma_n \times \tan\phi \quad (2)$$

where c and ϕ are cohesion and friction angle. Figure 10 compares the peak and residual shear strengths obtained from the first through the tenth cycles. The shear strengths of the smooth saw-cut fractures are also incorporated. Good correlations between the test results and the Coulomb criterion are obtained. The coefficient of correlations (R^2) for all curves are greater than 0.9. It is clear that the peak shear strengths of the second through tenth cycles for all rock types are notably lower than those of the first cycle. The reduction of these shear strengths is reflected by both cohesion and friction angle. The τ-σ_n diagrams in Figure 10 show that the shear strengths of the smooth saw-cut fractures are lower than the residual strengths. This implies that the second order asperities remain on the fracture planes after the first order asperities have been sheared off by the first shear cycle.

To further examine the variation of the peak and residual shear strengths, the friction angle and cohesion values calculated as a function of shear load cycles (N_s) are plotted in Figure 11. The results show that some variations

Table 1. Joint roughness coefficients of tested rocks.

Rock types	JRC	
	Before 1st cycle	After 10th cycle
PPSS	8-10	4-6
TGR	10-12	8-10
SLS	18-20	14-16

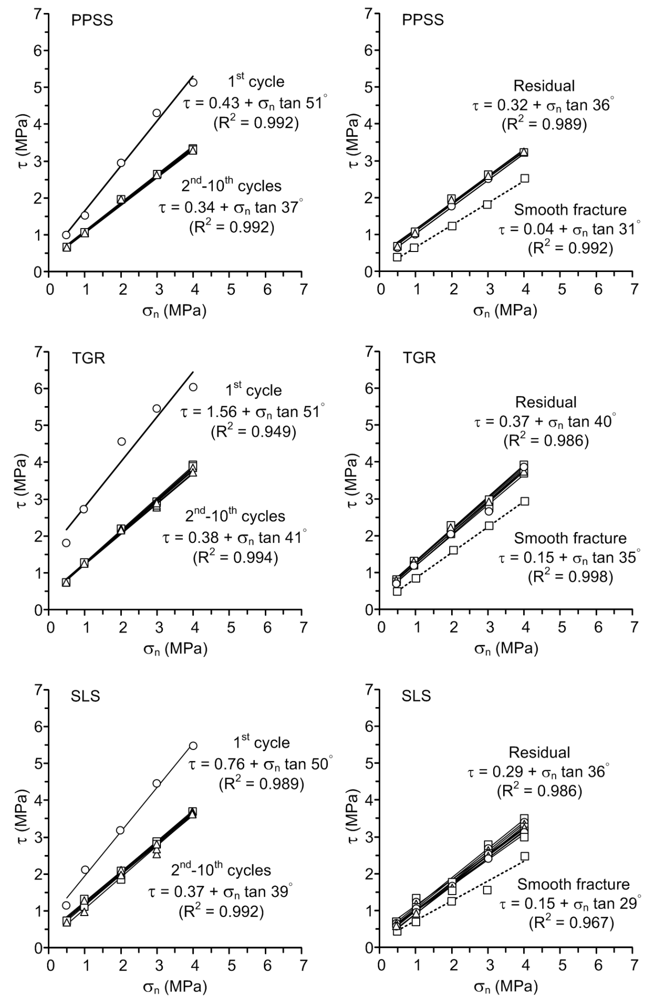

Figure 10. Shear strengths (t) as a function of normal stress (σ_n) for peak (a) and residual (b).

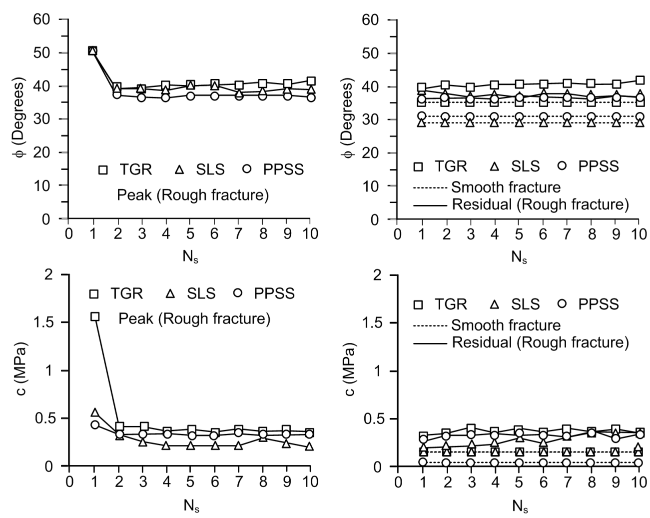

Figure 11. Friction angle and cohesion of peak (a) and residual (b) shear strengths as a function of number of shear cycles.

of the f and c values occur from the second through tenth cycles. In principle the residual f and c would continue to decrease as N_s increases, presumably due to the gradual degradation of the second order asperities. The fluctuation of these parameters is probably because the small rock fragments and powder trapped in the fracture aperture causes unequal effects on different shear cycles. The magnitudes of the residual f and c are nevertheless lower than those of the peak strengths and notably higher than those of the smooth fractures.

6. Discussions on Fracture Roughness Degradation

Table 2 summarizes the fracture characteristics at the 1st-cycle and the 10th-cycle. The peak and residual cohesions and friction angles of the 1st-cycle are higher than those of the 10th-cycle. The peak shear strengths significantly drop from the 1st-cycle to the 10th-cycle for all rock types. The residual shear strengths, however, are not that much different from the 1st-cycle through the 10th-cycle. It seems that fractures in softer rock (sandstone with lower UCS) tend to show larger reduction of the shear strengths than those of the stronger rocks (granite and limestone), as shown in Table 2. The fracture shear stiffness (K_s) tends to be insensitive to the rock strength. This is because the stiffness is mainly governed by the rigidity modulus of the fracture wall rock and by the cohesive force between two contact surfaces. The highest fracture shear stiffness is obtained from granite and limestone where they also have higher value of cohesion from the smooth fracture (see Figure 9) and higher intact strengths (see Table 2), compared to those of sandstone.

Since the precision of the laser scanning system used here is inadequate to directly measure the asperity angles, an indirect assessment of these angles is used. The Patton fracture shear strength (Hoek and Bray, 1981) concept is adopted to determine the 1st- and 2nd-orders of the asperities. Patton states that the friction angle of rock fracture may be separated into two parts: (1) basic friction angle (or friction angle of smooth surface), and (2) asperity angles. From Figure 10 the 1st-order asperity angle can, therefore, be approximated by subtracting the peak friction angle by the average residual friction angle. This is based on an assumption that the 1st-order asperity angle is completely sheared off after the 1st-shear cycle and leaves the 2nd-order asperity angle on the fracture surface. Subsequently the 2nd-order asperity angle can be approximated by subtracting to average residual friction angle by the friction angle of the smooth fracture. The results from these postulations are given in Table 3. Note that the 1st-order asperity angles are significantly greater than the 2nd-ones for all rock types. The largest difference is observed from the fractures in sandstone. This agrees with the JRC values measured before the 1st-cycle and after the 10th-cycle that the sandstone also shows the largest difference of the JRC values from the two measurements, as compared to those of the granite and lime-

Table 2. Characteristics of tension-induced fractures.

Rock types	USC (MPa)	Cycle	ϕ_p (degrees)	c_p (MPa)	ϕ_r (degrees)	c_r (MPa)	K_s (MPa/mm)	d_n/d_s
PPSS	85	1^{st}	51	0.43	37	0.27	2.3-6.0	0.30-0.14
		10^{th}	37	0.34	37	0.32	1.4-3.3	0.15-0.04
TGR	118	1^{st}	51	1.56	40	0.31	2.8-6.5	0.40-0.10
		10^{th}	41	0.38	40	0.35	1.2-3.6	0.16-0.06
SLS	93	1^{st}	50	0.76	39	0.21	2.3-6.2	0.40-0.14
		10^{th}	39	0.37	37	0.36	0.9-3.2	0.2-0.004

Table 3. Asperity angles approximated from friction angles.

Rock types	First order (i_{1st}) (degrees)	Second order (i_{2nd}) (degrees)
PPSS	15	5
TGR	11	5
SLS	14	7

stone. The 2nd-order asperity angles gradually reduce as the fractures roughness continues to degrade from the 2^{nd}-cycle through the 10^{th}-cycle which is also reflected by the gradual decrease of the residual friction angles.

7. Conclusions

This study clearly shows that the cyclic shear loading do affect the shear strengths and stiffness of rough fractures in sandstone, granite and limestone. The decrease of the peak shear strengths is due to the rapid degradation of the first order asperities during the first shear cycle, and the gradual degradation of the second order asperities during the second through tenth cycles. Here, the Coulomb criterion can well describe the peak and residual shear strengths of the rough and smooth fractures. The cohesion and friction angle of all rocks tested rapidly decrease from the first cycle and tend to remain constant through the tenth cycles. The joint shear stiffness also exponentially decreases with increasing loading cycles. The shear strengths of the smooth saw-cut fractures are clearly independent of the loading cycles. This suggests that for the same rock type the effects of cyclic shear loading may act more for rougher fractures with relatively low strength. It can therefore be postulated that the effect of cyclic shear may be found in other rock types that have comparable mechanical properties to those used in this study.

The τ-σ_n diagrams plotted in Figure 10 are useful for engineering applications. The results suggest that application of the peak shear strength (obtained from the first cycle) for the stability evaluations and design of slope embankments in the seismic activity areas may not be conservative. The peak and residual shear strengths obtained from the second through tenth cycles would be more appropriate in this case. The application of the shear strengths obtained from the smooth saw-cut fractures would be overly conservative for most engineering structures in rock mass under seismic activities.

Acknowledgements

This study is funded by Suranaree University of Technology and by the Higher Education Promotion and National Research University of Thailand. Permission to publish this paper is gratefully acknowledged.

References

ASTM Standard C127-12. 2014. Standard test method for density, relative density (specific gravity), and absorption of coarse aggregate. Annual Book of ASTM Standards, American Society for Testing and Materials, West Conshohocken, Pennsylvania, U.S.A.

ASTM Standard D5607-08. 2008. Standard test method for performing laboratory direct shear strength tests of rock specimens under constant normal force. Annual Book of ASTM Standards, American Society for Testing and Materials, West Conshohocken, Pennsylvania, U.S.A.

Barton, N. 1982. Shear strength investigations for surface mining. Proceedings of the 3rd International Conference on Surface Mining, Vancouver, Canada, 1982, 171-196.

Boonbatr, A. and Fuenkajorn, K. 2011. Design and analysis of adit for limestone quarry of Siam city cement public company limited. Proceedings of the 3rd Thailand Symposium on Rock Mechanics, Hua Hin, Thailand, March 10-11, 2011.

Brown, E.T. 1981. Rock characterization, testing and monitoring-ISRM suggested methods. Pergamon, Oxford, U.K., pp. 171-183.

Hoek, E. and Bray, J.W. 1981. Rock Slope Engineering, 3th edition, Taylor and Francis, New York, U.S.A.

Hosseini, K.A., Pellet, F., Jafari, M.K. and Boulon, M. 2004. Shear strength reduction of rock joints due to cyclic loading. Proceedings of the 13th World Conference on

Earthquake Engineering, Vancouver, Canada, August 1-6, 2004.

Hutson, R.W. and Dowding, C.H. 1990. Joint asperity degradation during cyclic shear. International Journal of Rock Mechanics and Mining Sciences Geomechanics Abstracts. 27(2), 109-119.

Jaeger, J.C., Cook, N.G.W. and Zimmerman, R.W. 2007. Fundamentals of Rock Mechanicals, 4th edition, Blackwell Publishing, Australia, pp. 475.

Jafari, M.K., Hosseini, K.A., Boulon, M., Pellet, F., Jalaly, H., Uromeihy, A. and Buzzy, O. 2002. Laboratory investigation on shear strength variation of joint replicas due to low and high amplitude cyclic displacements. JSEE: Summer and Fall. 4(2-3), 37-49.

Jafari, M.K., Hosseini, K.A., Pellet, F., Boulon, M. and Buzzy, O. 2003. Evaluation of shear strength of rock joints subjected to cyclic loading. Soil Dynamics and Earthquake Engineering. 23, 619–630.

Kenkhunthod, N. and Fuenkajorn, K. 2009. Loading rate effects on strength and stiffness of sandstones under confinement. Proceedings of the 2nd Thailand Symposium on Rock Mechanics, Chonburi, Thailand, March 12-13, 2009, 271-282.

Lee, H.S., Park, Y.J., Cho, T.F. and You, K.H. 2001. Influence of asperity degradation on the mechanical behavior of rough rock joints under cyclic shear loading. International Journal of Rock Mechanics and Mining Sciences. 38(7), 967-980.

Rodklang, K. and Fuenkajorn, K. 2014. Effects of temperatures on strength and deformability of Tak granite. Proceedings of the Conference on Advances in Civil Engineering for Sustainable Development, August 27-29, 2014.

Wendai, L. 2000. Regression analysis, linear regression and probit regression, In 13 chapters. SPSS for Windows: statistical analysis: Publishing House of Electronics Industry, Beijing, China.